SASEC2015
Third Southern African Solar Energy Conference
11 – 13 May 2015
Kruger National Park, South Africa

TOWARD HIGH-EFFICIENCY HYBRID (ELECTRICITY AND HEAT) HIGH-CONCENTRATION PHOTOVOLTAIC SYSTEMS

Severin Zimmermann[a,b], Henning Helmers[c], Manish K. Tiwari[a], Stephan Paredes[b], Bruno Michel[b], Maike Wiesenfarth[c], Andreas W. Bett[c], Dimos Poulikakos[*a]
[*]Author for correspondence
[a]Department of Mechanical and Process Engineering,, ETH Zurich, 8092 Zurich, Switzerland
[b]Advanced Thermal Packaging, IBM Research – Zurich, 8803 Rueschlikon, Switzerland
[c]Fraunhofer Institute for Solar Energy Systems ISE, 79110 Freiburg, Germany
[*]E-mail: dpoulikakos@ethz.ch

ABSTRACT

Photovoltaic power generation is a growing renewable primary energy source, expected to assume a major role as we strive toward fossil fuel free energy production. However, the rather low photovoltaic efficiencies limit the conversion of solar radiation into useful power output. Hybrid systems extend the functionality of concentrating photovoltaics (CPV) from simply generating electricity, to providing simultaneously electricity and heat. The utilization of otherwise wasted heat significantly enhances the overall system efficiency and boosts the economic value of the generated power output. The system presented in this lecture is the outcome of collaborative research in my research group, with the IBM research lab in Zurich and the Fraunhofer Institute for solar energy systems in Freiburg, Germany. It consists of a scalable hybrid photovoltaic-thermal receiver package, cooled with an integrated high performance microchannel heat sink we initially developed and optimized for the efficient cooling of electronics. The package can be operated at elevated temperatures due to its overall low thermal resistance between solar cell and coolant. The effect of the harvested elevated coolant temperature on the photovoltaic efficiency is investigated. The higher-level available heat can be suitable for sophisticated thermal applications such as space heating, desalination or cooling (polygeneration approaches). A total hybrid conversion efficiency of solar radiation into useful power of 60% has been realized. The exergy content of the overall output power was increased by 50% through the exergy content of the extracted heat.

INTRODUCTION

The energy demand of the world is continuously rising due to ever increasing global population and industrialization [1]. At present, energy from non-renewable resources such as fossil fuels or fissionable materials accounts for over 92% of the world energy usage [2]. In addition, energy generation based on burning of fossil fuels has caused an increase in carbon dioxide (CO2) and other greenhouse gas emissions, leading to global warming. A switch from fossil fuels to renewable energy sources such as sun, wind or water has become one of the major challenges of the 21st century. Harvesting solar energy is a promising technology for renewable power generation with the potential to meet a significant proportion of the world's energy needs. There are many alternatives available to directly harness the sun's energy, the most prevalent of which are solar collectors designed to generate thermal energy and photovoltaic cells generating electricity, the latter being the main focus in this paper.

However, generating electric power from solar radiation through photovoltaic conversion is dominated by technologies using one material for the solar cell. This approach limits the conversation efficiency to about 25%. Although highest efficiencies can be reached using multi-junction solar cells [3] their fabrication costs still pose a limiting factor. Therefore, in concentrating photovoltaic (CPV) systems the sunlight is collected by concentrating optics and focused onto a considerably smaller photovoltaic receiver. Thus, this technology substitutes expensive photovoltaic cell material by inexpensive optical equipment. This approach reduces the cost per produced kilowatt-hour [4-5]. Some of the first concentrator systems used Fresnel lenses [6] or compound parabolic concentrators [7] to achieve concentration of the sunlight. Higher concentrations of up to 1000 suns were mainly achieved through the use of solar tower reflectors in the center of multiple heliostats [8] and parabolic dish based systems [5, 9-11]. The latter are suitable for various applications ranging from small rooftop photovoltaic power stations to high concentration photovoltaic thermal systems with concentration of 2000 suns [12].

Despite very different designs, all solar concentrator systems share some key requirements. Thermal management and temperature control are among the most important aspects in any concentrator system because of the generated high power densities. Especially CPV systems require strict temperature

control because of the strong influence of the operation temperature on the photovoltaic conversion process. The electrical efficiency and, consequently, the power output of a photovoltaic module depend linearly on the operating temperature [13]. High concentration ratios impact the system performance in several ways. First, photovoltaic efficiency increases with increasing irradiance (up to a design specific limit) [14]. Second, high concentration involves high heat fluxes and, consequently, the design of the heat exchanger and the selection of an appropriate coolant become of paramount importance [15]. However, increasing concentration reduces the influence of temperature on photovoltaic efficiency [16-20]. If high concentrating photovoltaic (HCPV) systems were to serve as viable source to appreciably meet the global energy demand, a systemic approach addressing the high efficiency requirements and potential of both the photovoltaic and cooling components is needed. Despite high photovoltaic conversion efficiencies, more than 50% of the potential power output is dissipated as heat. Therefore, advancements with respect to overall solar energy collection and usage of the heat in photovoltaic systems will boost the overall energy efficiency significantly. Photovoltaic thermal collectors have been investigated intensively for lower concentrations and it has been shown that this approach significantly enhances the efficiency [21-22].

The current work investigates a hybrid High Concentration Photovoltaic-Thermal (HCPVT) system designed to achieve optimal overall module efficiency. This includes the maximal generation of electricity and the associated harvesting of produced thermal power enabling its further utility. A related system has been modeled previously to look at multi junction solar cells in a solar concentration energy system with active cooling [23]. The thermal requirements of these hybrid solar receivers are very similar to micro processors in high performance computing. To this end, the recently demonstrated technologies for energy management in high performance computing [24-25] can be integrated synergistically in HCPVT systems. Approaches for reuse of otherwise wasted heat demonstrated in supercomputers [26] and datacenters [27-28] can be used to boost the energy efficiency on in HCPVT systems. The operating temperature of the PV cells is controlled to allow direct reuse of the collected heat at the required temperature level, and is simultaneously kept low-enough to maintain high electrical efficiency. A direct reuse of heat from HCPVT systems targets the replacement of heat generated by combustion of fossil fuels (also a wasteful approach in terms of exergy), thereby reducing the global carbon footprint.

The temperature of the wasted heat is pivotal to assess its value for potential reuse. In terms of exergetic content, thermal energy is inferior to electric energy, because it cannot be efficiently converted to mechanical energy (Carnot-limited conversion). Additionally, thermal energy carriers are usually difficult to transport. An exergy [29] analysis of any system can provide crucial information about the usefulness of the collected energy [30-32].

The present work focuses on the thermal characteristics of the photovoltaic package and includes a complete energy and exergy analysis of an experimental prototype rooftop photovoltaic power station based on a parabolic dish concentrator. The research lays a thermodynamic foundation for developing hybrid photovoltaic-thermal systems with integrated energy reuse and minimal carbon footprint.

NOMENCLATURE

A	[m^2]	Receiver Area ()
C	[-]	Concentration ratio
c_p	[J/kg K]	Specific heat capacity (J/kg K)
DNI	[W/m^2]	Direct normal irradiance ()
EEVC	[-]	Enhanced economic value coefficient
$\dot{E}x$	[W]	Exergy (W)
h	[J/kg]	Enthalpy (J/kg)
$\dot{m}$	[kg/s]	Mass flow rate (kg/s)
P	[W]	Power (W)
$\dot{Q}$	[W]	Heat (W)
R_{th}	[K/W]	Thermal resistance (K/W)
s	[J/kg K]	Entropy (J/kg K)
T	[K]	Temperature (K)
U	[-]	Utility function

Greek letters

Δ	Difference between inlet and outlet
η	Efficiency
χ	Price for 1 kWh of energy

Subcripts

0	Reference from ambient
comb	Combined (electrical and thermal)
el	Electric
ff	Fossil fuels
in	inlet
max	Maximum
MP	at the maximum point
out	Outlet
pump	Pump
Sol	Solar
sun	Sun
th	Thermal

EXPERIMENTAL SETUP

The investigated setup and its different components are shown in Figure 1. A description of the different components and their characteristics is presented in the sequel.

2.1 Photovoltaic converter

A single-junction GaAs monolithic interconnected module (MIM) solar cell was chosen for a proof of principle demonstration. MIMs consist of several photovoltaic cell segments, which are series-connected during cell fabrication process [33-34]. In this approach the photovoltaic area is divided in several series-connected segments leading to a high voltage and low current device. Because of the low current, power losses due to series resistances can be kept small. The applied MIM consisted of 23 solar cell segments. Each segment of the MIM was protected by a bypass diode which is

monolithically integrated into the semiconductor layer structure [34]. The total area of the MIM cell was 4.33 cm^2.

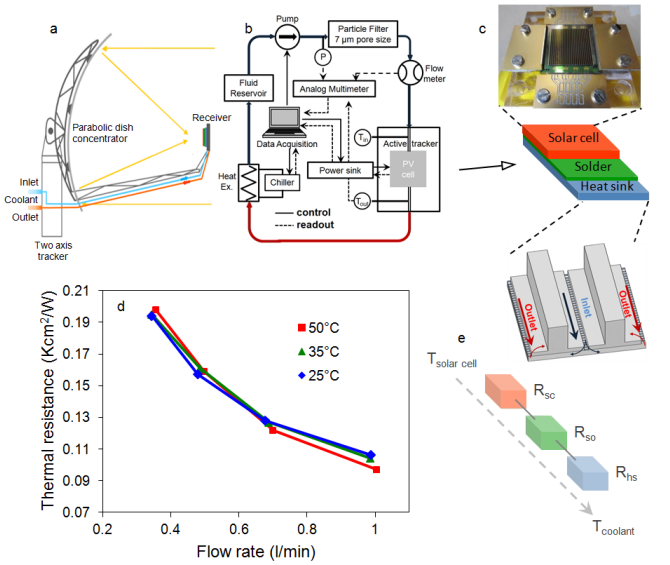

Figure 1: Photovoltaic receiver system and its thermal characteristics. (a) Scheme of the parabolic dish concentrator. (b) Schematic of the experimental outdoor test facility. (c) Photograph and model of the photovoltaic receiver package highlighting the top view.

Receiver package

The MIM cell was bonded to a manifold microchannel heat sink, enabling the efficient heat removal from its backside. A model of the receiver package is shown in Figure 1c. The bonding was performed by using a vacuum assisted solder process to obtain a void free solder layer. Voids in the solder layer need to be avoided, because they create local hotspots and unwanted thermal stress resulting in degradation of thermal performance. A detailed design of the microchannel heat sink has been reported elsewhere [24].It consists of a manifold layer that feeds a heat transfer structure of hundreds of parallel microchannels as shown in the lower part of Figure 1c. The coolant enters the manifold system laterally and branches into several inlet channels. Afterwards, the liquid is guided into the underlying level of heat transfer enhancing microchannels. While moving along the microchannels, which are orthogonally orientated with respect to the manifold, the liquid removes the heat generated by the receiver. Subsequently, the liquid leaves the microchannel structure upwards into the outlet channels before it is guided to a lateral outlet.

Four resistance temperature detectors (RTD) were placed between the photovoltaic cell and the heat sink to estimate the MIM cell temperature and to evaluate the thermal resistance of the entire package.

2.3 HCPVT system

The receiver package was mounted on an outdoor active-tracking system (scheme is shown in Figure 1a) with a tracking accuracy of 0.12°. The sunlight was concentrated on the receiver with a parabolic dish concentrator having a concentration ratio of approximately 500. A flux homogenizer was installed to help smooth-out the irradiation irregularities from the parabolic dish [35-36]. The receiver package was connected to a fluid loop shown in Figure 1b, to allow precise temperature control. The flow was driven by a magnetic gear pump and a coriolis flow meter determined the volumetric flow rate with an error of ±10 ml/min. Two cross calibrated T-type thermocouples measured the fluid inlet and outlet temperatures of the receiver package (error ±0.1 K). Another thermocouple was used to measure the ambient temperature. The fluid inlet temperature was controlled with a heat exchanger connected to a chiller. A 7 µm pore filter (Swagelok, USA) was used to keep the coolant (water) free of large particles and prevent any clogging of the microchannels in the heat sink. The direct normal irradiance (DNI) was measured by a pyrheliometer mounted on the solar tracker, while the global horizontal irradiance (GHI) was recorded by a pyranometer on the roof. A programmable DC electronic load was used to measure the I-V characteristics of the solar cell. The data acquisition was performed by a digital multimeter and a relay switching card. The system operation and data recording were performed with LabVIEW®. The entire test facility was installed in Zurich, Switzerland. A comparable setup is located at Fraunhofer ISE in Freiburg, Germany [37].

The irradiance distribution in the receiver plane was measured using a solar flux sensor (circular active area of 12 mm^2) mounted on a three axis (3D) translation stage. The 3D stage was used to move the flux sensor in order to create a grid of data points spaced at intervals of 5 mm in width and height (linear interpolation was performed in between).

RESULTS AND DISCUSSION

Thermal characteristics of the heat sink

The key parameter used to describe the thermal performance of a heat sink is the thermal resistance. Thermal resistance is a measure for the temperature difference between the solar cell and the coolant needed to remove a given amount of generated heat

$$R_{th} = \frac{\Delta T}{\dot{Q}} \quad (1)$$

The total thermal resistance of the receiver package can be split into three components connected in series as shown in Figure 1e. The first component originates from the solar cell itself, because the generated heat passes through the cell's semiconductor layers and is removed from its backside. This component of the thermal resistance is a function of the thermal conductivity of the materials involved and their thickness. The second resistance emerges due to the solder interface connecting the solar cell and the heat sink and mainly depends on the solder material as well as the existence of voids in the interface layer. The third part of the thermal resistance is due to the heat sink, and is a function of the geometry as well as the material properties of the heat sink [24] and the characteristics of the coolant such as flow rate [38]. The thermal resistance of

the solder interface and the heat sink was measured using the four RTD sensors between solar cell and heat sink. The resulting overall thermal resistance is plotted in Figure 1d at different coolant flow rates and the coolant inlet temperatures. The thermal resistance decreases for higher flow rates due to an enhancement in convective heat transfer. However, the thermal resistance does not change significantly as a function of the coolant inlet temperature. The thermal conductivity of solid materials decreases for higher temperatures causing an increase in the resistance. This is matched by an increase of the thermal conductivity and the specific heat of the cooling water at higher temperatures resulting in a decrease of the combined thermal resistance. The two competing effects almost cancel each other out. The thermal resistance of the solar cell could not be measured because the installation of additional RTD sensors on top of the solar cell would have resulted in a loss of active area thereby decreasing the overall performance. Instead, the thermal resistance of the solar cell was approximated to be equal to a layer of GaAs of the same thickness. The resulting total thermal resistance of the receiver package for a coolant flow rate of 1 l/min was approximately 0.2 Kcm^2/W corresponding to a 20˚C temperature difference between solar cell and coolant for a concentration of 1000 suns (1 sun = 0.1 W/cm²).

Preliminary solar cell characterization

The electrical performance of the solar cell was determined with current-voltage characteristics (I-V curves) for a coolant inlet temperature of 25°C under different intensities. The characterization was performed indoors at a flash sun simulator under homogeneous illumination. Variation of the distance between flash bulb and solar cell enables variation of the light intensity in the measurement plane. Figure 2a shows the I-V curves at different concentration ratios. At a concentration ratio of 489, the electrical efficiency is 20.0%.

Outdoor performance

Indoor measurements are necessary to determine the optimal performance of solar cells, because the testing conditions are precisely controllable. However, outdoor measurements are crucial to determine the realistic effects of the changing conditions due to wind and cloud movement, movement of the tracker, etc.
Figure 2b shows the measured I-V data of the solar cell from outdoor testing. The overall open circuit voltage is given by the superposition of the open circuit voltages of the individual segments. A detailed analysis of such results with respect to homogenization effects effects can be found in [36].

The inhomogeneous illumination was confirmed by measuring the irradiance distribution across the solar cell plane. Variations in illumination concentration from 200 to 550 were observed with two hotspots in the middle and zones with low concentration on the right and the left sides. The receiver is located in the center of the measured concentration field. There, the variation is considerably lower and ranges from 400 to 550 suns.

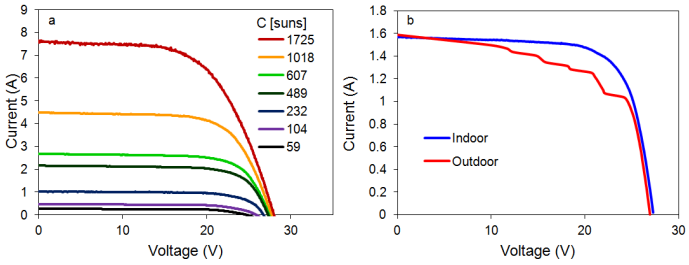

Figure 2: (a) I-V curves of the receiver measured indoors at a flash sun simulator under different concentration ratio C. (b) Comparison of I-V curves of the receiver measured indoors/outdoors. The standard DNI for indoor measurement is 1000 W/m^2 whereas the outdoor DNI was measured to be between 850 W/m^2 and 920 W/m^2.

The electric efficiency of the receiver is given by:

$$\eta_{el} = \frac{P_{\mathrm{MP}}}{C \cdot DNI \cdot A} \qquad (2)$$

where A=4.33 cm² is the receiver area, DNI is the measured direct normal irradiance, C denotes the corresponding averaged concentration ratio across A as described above, and PMP is the maximal electrical power. Essentially, Eq. (2) expresses the 1st law efficiency for the electrical component of the generated energy.
The thermal power Pth is determined from a simple caloric computation based on the temperature rise of the coolant water flowing from inlet to outlet ΔT, the mass flow $\dot{m}$ and the specific heat capacity of the coolant c_p:

$$P_{th} = \dot{m} c_p \Delta T \qquad (3)$$

The hybrid efficiency of the system, while operating at maximum electrical power output, is then given by:

$$\eta_{comb} = \frac{P_{\mathrm{MP}} + P_{th}}{C \cdot DNI \cdot A} \qquad (4)$$

The measured energy efficiency curves both for the case where only electrical power is considered and for case where combined electrical and thermal power generation are considered jointly are shown in Figure 3a. An increase of the cell temperature results in a minor drop of 0.02 %K-1 of the electric efficiency within the investigated temperature range. The thermal efficiency decreases more distinctly with increasing temperature due to increasing thermal losses to the ambient. The drop in thermal energy recovery efficiency is 0.1 $\%K^{-1}$. The inclusion of the thermal energy in the hybrid efficiency boosts the value to 60% at 25°C inlet temperature. This corresponds to a 400% increase in energy efficiency compared to the purely electric efficiency of this specific solar cell. The energy flow can also be conveniently expressed through a Sankey diagram [39]. Figure 3b shows the

corresponding diagram for the present HCPVT system in hybrid operation for a coolant inlet temperature of 60°C. The incoming solar power is partially converted into electric power and heat in the PV cell. A fraction of the generated heat at the level of the PV cell is lost to the environment via radiative and convective heat transfer. However, due to the efficient cooling most of the heat is removed by the coolant and can be utilized in a secondary application.

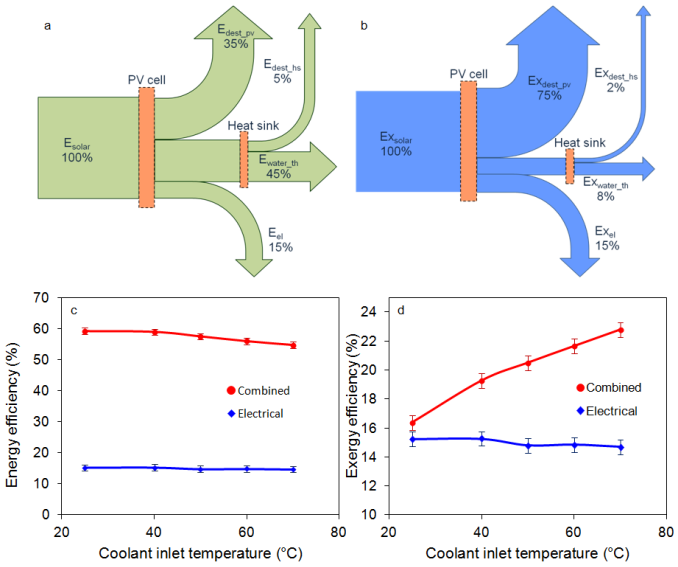

Figure 3: (a) Sankey diagram of the energy flow across the photovoltaic receiver. The subscripts th, el and dest respectively denote thermal energy, electrical energy and energy losses. (b) Sankey diagram of the exergy flow across the photovoltaic receiver. (c) Energy efficiency of the photovoltaic receiver for electrical and combined electrical/thermal operation as a function of the coolant inlet temperature. (d) Energy efficiency of the photovoltaic receiver for electrical and combined electrical/thermal operation as a function of the coolant inlet temperature.

Exergy analysis

To evaluate the usefulness of the thermal energy that is extracted from the receiver, an exergy analysis is performed. Exergy is a thermodynamic property, and as it is known, it represents the maximum useful work potential that is contained in an amount of energy. The exergy input from solar irradiation, Ex_{Sol}, can be calculated using the Petela[40] expression as:

$$\dot{E}x_{Sol} = DNI \cdot A\left[1-\frac{4}{3}\left(\frac{T_o}{T_{sun}}\right)+\frac{1}{3}\left(\frac{T_o}{T_{sun}}\right)^4\right] \quad (5)$$

where T_{sun} is the temperature of the sun (6000 K) and To the ambient temperature (293 K). The Petela expression essentially acts as an optical efficiency for the conversion of radiation into useful work. Electrical energy generated by the photovoltaic cell is considered pure exergy, whereas the exergy content of the thermal energy is typically low (Carnot limit). The exergy content of thermal energy recovered in our combined solar cell and cooling module Ex_{th}, can be written as [29]

$$\dot{E}x_{th} = \dot{m}\left[h_{out}-h_{in}-T_o\left(s_{out}-s_{in}\right)\right] \quad (6)$$

where h and s denote the specific enthalpy and entropy of the coolant and subscripts 'out', 'in' and '0' denote the outlet, inlet and reference ambient conditions, respectively. The exergy content of the extracted heat increases with temperature underscoring the main benefit of high temperature operation. The exergy analysis can help to identify sites where exergy losses occur, and rank them according to their significance so as to provide guidelines for a more efficient system design with better energy recovery efficiency. The exergy flow was plotted in the same way as the energy flow in a Sankey diagram for a coolant inlet temperature of 60ºC in Figure 3c Approximately 15% of the initial exergy is converted into electricity. The major part of the initial exergy is converted into heat. The conversion from radiation to heat already accounts for an exergy loss of 85% of the initial value for a water inlet temperature of 25°C. The loss decreases to 75% for a water inlet temperature of 70°C. This loss could be further reduced through operation at even higher temperatures. 15% of the initial exergy is available as electricity whereas the rest of the exergy is available as thermal energy. Due to an inevitable temperature differential, further exergy destruction occurs during the heat transfer in the water flowing through the heat sink. Finally, 8.5% of the exergy is transferred to the water for a water inlet temperature of 70°C. From Figure 3b it is clear, that the largest exergy destruction occurs in the photovoltaic cell. One way to decrease the exergy destruction is to increase the photovoltaic cell efficiency. One way to enhance the efficiency for a given solar cell is to cool them down to low temperatures albeit this counteracts the potential benefits of direct reuse of the thermal energy in HCPV systems. The best way to optimize the overall module efficiency is to achieve a compromise between maximal electricity generation and thermal energy reuse.

In hybrid operation, where the thermal energy gained by the coolant is also utilized, the total exergy output is increased by 55% when the coolant inlet temperature is increased from 25 °C to 70 °C. We can introduce the following exergy-based, second law efficiency for the heat sink, to point out the importance of the different exergy inputs and outputs

$$\eta_{2^{nd}} = \frac{\dot{E}x_{th}+\dot{E}x_{el}}{\dot{E}x_{Sol}+P_{pump}} \quad (7)$$

where Ex_{el} denotes the electric power generated by the photovoltaic cell. P_{pump} denotes the (parasitic) pumping power needed to drive the coolant through the microchannel heat sink. In our setup, the pumping power was negligible compared to the other terms. In Figure 3d the exergy efficiency (2nd law efficiency) is plotted as a function of the coolant inlet temperature. The exergy efficiency for the combined case increases up to 60% compared to the purely electrical case with

increase in the water inlet temperature from 25 to 70°C. From this behaviour, it is clear that in order to maximize the exergy efficiency, the water inlet temperature should be maximized up to a photovoltaic cell temperature that does not significantly affect the electrical performance of the receiver. The trends of the 1st and 2nd law efficiencies are reversed. The higher 1st law efficiency for low coolant temperatures does not guarantee a high 2nd law efficiency and vice versa. Energy losses to the ambient and a lower electric efficiency for even higher coolant temperatures will become significant, thereby also limiting the 2nd law efficiency. It is worth mentioning that, in addition to the thermodynamic efficiency, economic considerations accounting for the geographic specificity of the area of application of the technology must be also taken into account [43].

ACKNOELEDGEMENTS

We acknowledge the financial support by the ETH Zurich, by the IBM First-Of-A-Kind (FOAK) program, and by the Swiss Center of Competence for Energy and Mobility (CCEM). The development of the MIM technology at Fraunhofer ISE was supported by the Federal Ministry for the Environment, Nature Conservation and Nuclear Safety (BMU) under the "KoMGen" Project (#0327567A). The authors thank Werner Escher, Pedro Neves and Ute Drechsler for their contribution in the manufacturing of the receiver package. We also thank Elvira Fehrenbacher and Michael Schachtner for their support with the indoor measurements.

REFERENCES

[1] Wolfram C, Shelef O, Gertler P. How Will Energy Demand Develop in the Developing World? Journal of Economic Perspectives. 2012;26:119-38.
[2] Primary energy, Statistical Review of World Energy 2012. BP Global; 2012.
[3] Green MA, Emery K, Hishikawa Y, Warta W, Dunlop ED. Solar cell efficiency tables (version 42). Progress in Photovoltaics. 2013;21:827-37.
[4] Faiman D, Biryukov S, Pearlmutter KK, Ieee I. PETAL: A research pathway to fossil-competitive solar electricity2002.
[5] Verlinden PJ, Lewandowski A, Bingham C, Kinsey GS, Sherif RA, Lasich JB, et al. Performance and reliability of multijunction III-V modules for concentrator dish and central receiver applications. Conference Record of the 2006 IEEE 4th World Conference on Photovoltaic Energy Conversion, Vols 1 and 2. New York: Ieee; 2006. p. 592-7.
[6] Nakata Y, Shibuya N, Kobe T, Okamoto K, Suzuki A, Tsuji T. PERFORMANCE OF CIRCULAR FRESNEL LENS PHOTO-VOLTAIC CONCENTRATOR. Japanese Journal of Applied Physics. 1980;19:75-8.
[7] Winston R. Development of the compound parabolic collector for photo-thermal and photo-voltaic applications. Proceedings of the Society of Photo-Optical Instrumentation Engineers Vol68 Optics in Solar Energy Utilization. 1975:136-44.
[8] Ittner Iii WB. An array of directable mirrors as a photovoltaic solar concentrator. Solar Energy. 1980;24:221-34.
[9] Polonsky G, Shelef G, Flitsanov Y, Wiesenfarth M, Steiner M, Helmers H, et al. Efficiency of dense-array CPVT module with front-side interconnected cells. 9th International Conference on Concentrator Photovoltaic Systems. Miyazaki, Japan2013.
[10] Chayet H, Kost O, Moran R, Lozovsky I. Efficient, Low Cost Dish Concentrator for a CPV Based Cogeneration System. In: Dimroth F, Kurtz S, Sala G, Bett AW, editors. 7th International Conference on Concentrating Photovoltaic Systems2011.
[11] Helmers H, Kramer K. Multi-linear performance model for hybrid (C)PVT solar collectors. Solar Energy. 2013;92:313-22.
[12] IBM Research Zurich. Made in IBM Labs: Collaboration Aims to Harness the Energy of 2,000 Suns. Zurich2013.
[13] Skoplaki E, Palyvos JA. On the temperature dependence of photovoltaic module electrical performance: A review of efficiency/power correlations. Solar Energy. 2009;83:614-24.
[14] Helmers H, Bett AW, Parisi J, Agert C. Modeling of concentrating photovoltaic and thermal systems. Progress in Photovoltaics: Research and Applications. 2014;22:427-39.
[15] Royne A, Dey CJ, Mills DR. Cooling of photovoltaic cells under concentrated illumination: a critical review. Solar Energy Materials and Solar Cells. 2005;86:451-83.
[16] Siefer G, Bett AW. Analysis of temperature coefficients for III–V multi-junction concentrator cells. Progress in Photovoltaics: Research and Applications. 2014;22:515-24.
[17] Helmers H, Schachtner M, Belt AW. Influence of temperature and irradiance on triple-junction solar subcells. Solar Energy Materials and Solar Cells. 2013;116:144-52.
[18] Kinsey GS, Hebert P, Barbour KE, Krut DD, Cotal HL, Sherif RA. Concentrator multijunction solar cell characteristics under variable intensity and temperature. Progress in Photovoltaics. 2008;16:503-8.
[19] Nishioka K, Takamoto T, Agui T, Kaneiwa M, Uraoka Y, Fuyuki T. Annual output estimation of concentrator photovoltaic systems using high-efficiency InGaP/InGaAs/Ge triple-junction solar cells based on experimental solar cell's characteristics and field-test meteorological data. Solar Energy Materials and Solar Cells. 2006;90:57-67.
[20] Sewang Y, Garboushian V. Reduced temperature dependence of high-concentration photovoltaic solar cell open-circuit voltage (Voc) at high concentration levels. 1994 IEEE First World Conference on Photovoltaic Energy Conversion Conference Record of the Twenty Fourth IEEE Photovoltaic Specialists Conference-1994 (CatNo94CH3365-4). 1994:1500-4 vol.2.
[21] Coventry JS. Performance of a concentrating photovoltaic/thermal solar collector. Solar Energy. 2005;78:211-22.
[22] Calise F, Vanoli L. Parabolic Trough Photovoltaic/Thermal Collectors: Design and Simulation Model. Energies. 2012;5:4186-208.
[23] Kerzmann T, Schaefer L. System simulation of a linear concentrating photovoltaic system with an active cooling system. Renewable Energy. 2012;41:254-61.
[24] Escher W, Brunschwiler T, Michel B, Poulikakos D. Experimental investigation of an ultra-thin manifold microchannel heat sink for liquid-cooled chips. J Heat Transfer. 2010;132:081402.
[25] Escher W, Michel B, Poulikakos D. A novel high performance, ultra thin heat sink for electronics. International Journal of Heat and Fluid Flow. 2010;31:586-98.
[26] Brunschwiler T, Meijer GI, Paredes S, Escher W, Michel B. Direct waste heat utilization from liquid-cooled supercomputers. Proceedings of the 14th International Heat Transfer Conference. Washington2010. p. 23352.
[27] Zimmermann S, Tiwari MK, Meijer GI, Michel B, Poulikakos D. Aquasar: A hot water cooled data center with direct energy reuse. Energy. 2012;43:237-45.

[28] Brunschwiler T, Smith B, Ruetsche E, Michel B. Toward zero-emission data centers through direct reuse of thermal energy. IBM J Res & Dev. 2009;53:Paper 11.
[29] Moran MJ, Shapiro HN. Fundamentals of engineering thermodynamics. 6th ed. Hoboken: John Wiley & Sons; 2008.
[30] Rosen MA, Dincer I, Kanoglu M. Role of exergy in increasing efficiency and sustainability and reducing environmental impact. Energy Policy. 2008;36:128-37.
[31] Charalambous PG, Maidment GG, Kalogirou SA, Yiakoumetti K. Photovoltaic thermal (PV/T) collectors: A review. Appl Therm Eng. 2007;27:275-86.
[32] Fujisawa T, Tani T. Annual exergy evaluation on photovoltaic-thermal hybrid collector. Solar Energy Materials and Solar Cells. 1997;47:135-48.
[33] Helmers H, Oliva E, Bronner W, Dimroth F, Bett AW. Processing Techniques for Monolithic Interconnection of Solar Cells at Wafer Level. Ieee Transactions on Electron Devices. 2010;57:3355-60.
[34] Loeckenhoff R, Dimroth F, Oliva E, Ohm A, Wilde J, Faiman D, et al. Development, characterisation and 1000 Suns outdoor tests of GaAs monolithic interconnected module (MIM) receivers. Progress in Photovoltaics: Research and Applications. 2008;16:101-12.
[35] Ries H, Gordon JM, Lasken M. High-flux photovoltaic solar concentrators with kaleidoscope-based optical designs. Solar Energy. 1997;60:11-6.
[36] Helmers H, Thor WY, Schmidt T, van Rooyen D, Bett AW. Optical analysis of deviations in a concentrating photovoltaics central receiver system with a flux homogenizer. Applied Optics. 2013;52:2974-84.
[37] Helmers H, Boos A, Jetter F, Heimsath A, Wiesenfarth M, Bett AW. Outdoor Test Setup for Concentrating Photovoltaic and Thermal (CPVT) Systems. In: Dimroth F, Kurtz S, Sala G, Bett AW, editors. 7th International Conference on Concentrating Photovoltaic Systems2011.
[38] Incropera FP, DeWitt DP. Fundamentals of Heat and Mass Transfer. 5th ed: John Wiley & Sons, Inc.; 2002.
[39] Sankey Diagrams, A Sankey diagram says more than 1000 pie charts. 2013.
[40] Petela R. Exergy of undiluted thermal radiation. Solar Energy. 2003;74:469-88.
[41] Energy prices and costs in Europe. Communication from the Commission to the European Parliament, the Council , and the European Economic and Social Committee and the committee of the Regions. Brussels 2014. p. 6-8.
[42] EKZ. Tarife Gewerbe, bis 100'000 kWh. 2011.
[43] Zimmermann S. et al. Toward High Efficiency, Hybrid, High-Concentration Photovoltaic Systems, under review, (2014.)